Journal of Molecular Graphics and Modelling 47 (2014) 8–17

Contents lists available at ScienceDirect

Journal of Molecular Graphics and Modelling

journal homepage: www.elsevier.com/locate/JMGM

# Insight into the interaction between DNA bases and defective graphenes: Covalent or non-covalent

Zhenfeng Xu, Biswa Ranjan Meher, Darnashley Eustache, Yixuan Wang*

*Computational Chemistry Laboratory, Department of Natural Sciences, Albany State University, Albany, GA 31705, USA*

ARTICLE INFO

*Article history:*
Accepted 14 October 2013
Available online 24 October 2013

*Keywords:*
DNA bases
Defective graphene
Noncovalent interaction
DFT-D

ABSTRACT

Although some metal clusters and molecules were found to more significantly bind to defective graphenes than to pristine graphenes, exhibiting chemisorptions on defective graphenes, the present investigation shows that the adsorption of DNA bases on mono- and di-vacant defective graphenes does not show much difference from that on pristine graphene, and is still dominantly driven by noncovalent interactions. In the present study the adsorptions of the nucleobases, adenine (A), cytosine (C), guanine, (G), and thymine (T) on pristine and defective graphenes, are fully optimized using a hybrid-meta GGA density functional theory (DFT), M06-2X/6-31G*, and the adsorption energies are then refined with both M06-2X and B97-D/6-311++G**. Graphene is modeled as nano-clusters of $C_{72}H_{24}$, $C_{71}H_{24}$, and $C_{70}H_{24}$ for pristine, mono- and di-vacant defective graphenes, respectively, supplemented by a few larger ones. The result shows that guanine has the maximum adsorption energy in all of the three adsorption systems; and the sequence of the adsorption strength is G > A > T > C on the pristine and di-vacant graphene and G > T > A > C on the mono-vacant graphene. In addition, the binding energies of the DNA bases with the pristine graphene are less than the corresponding ones with di-vacant defective graphene; however, they are greater than those of mono-vacant graphene with guanine and adenine, while it is dramatic that the binding energies of mono-vacant graphene with thymine and cytosine appear larger than those of pristine graphene.



## 1. Introduction

As one of the most recent interesting material due to its unique chemical and electronic properties [1], graphene has attracted wide attention to its promising applications in bio-medicine and micro-electronic devices. For example, nano-graphene has been proposed to make sensors for small molecules such as $H_2$, $H_2O$, NO, and $NH_3$ [2,3], and for biomolecules like carbohydrates, proteins, nucleic acids [4,5], and to convey drug and gene for cancer treatment [6]. Like carbon nanotubes [7,8], a major barrier for biomedical applications of nano-graphene is its low solubility in aqueous solutions. Strategic approaches toward solubilization of nanographene have been developed through non-covalent functionalization, which can not only enhance solubility of nanographene but also maintain its attractive geometric, electronic and mechanical properties. It is apparent that carbohydrates, proteins, and nucleic acids are very important species for functionalizing graphene in living systems.

With different models for pristine graphene, a variety of the first-principles based methods have been widely employed to investigate the binding of the nucleobases to pristine graphene, including local density approximation (LDA) type of density functional theory (DFT), GGA, meta-hybrid GGA, plane-wave GGA type of DFT, dispersion-corrected DFT (DFT-D) as well as second-ordor Møller–Plesset perturbation theory (MP2) [9–16]. Using B97-D, B2PLYP-D and SCS-MP2 methods, Antony et al. extensively investigated the adsorption of the DNA nucleobases on a variety of graphene clusters from 24 to 150 carbon atoms [10]. The interaction sequence after basis set superposition error correction (BSSE) at B2PLYP-D/TVZ(2df,2pd)//B97-D/TZV(d,p) level for DNA bases on $C_{54}H_{18}$ is, G (23.9 kcal/mol) > A (19.7) > T(18.5) > C(18.2), and they suggested the proper size of nano graphene with at least about 50 carbon atoms. MP2/6-311+G(d,p) results in the binding order of G(24.6 kcal/mol) > A(21.7 kcal/mol) ≈ *T*(21.4 kcal/mol) > C(18.4 kcal/mol) [9], parallel to the polarizability of the DNA bases. The plane-wave LDA method usually considerably underestimates the binding strength, like only 9.0 and 11.03 kcal/mol for cytosine [9,12]. Both the B3LYP-D/6-31G(d) with fifty five $C_6$ rings for graphene [14], and vdw-HF/6-31G(d,p) with twenty $C_6$ rings[11] reproduce the binding sequence, G > A > T > C, (17.5 > 15.0 > 14.3 > 13.3 kcal/mol; [14] 19.1 > 17.8 > 16.6 > 14.5 kcal/mol [11]); however, the absolute binding energies for the given base are a few kcal/mol lower than those predicted by the above B2PLYP-D method [10]. Van der Waals

* Corresponding author.
*E-mail address:* yixuan.wang@asurams.edu (Y. Wang).

1093-3263/$ – see front matter © 2013 Elsevier Inc. All rights reserved.
http://dx.doi.org/10.1016/j.jmgm.2013.10.007

density functional (vdW-DF) [17–19] for adenine on graphene also yields a too low binding (16.4 kcal/mol) [1,13], as compared to the result of Antony and Grimme (19.7 kcal/mol [10]). The binding energies from the wB97XD/6-31G(d,p) with 8 × 8-ring graphene sheet [16] agree very well within 0.1–1.4 kcal/mol with those of Antony et al. [10], yet the relative strength for T and C are switched (G > A > C > T, 22.5 > 20.3 > 18.9 and 18.4 kcal/mol). Varghese et al. carried out an experimental investigation into the binding of DNA nucleobases with graphene using isothermal titration calorimetry (ITC) [11]. They indicated that the relative interaction energies of the nucleobases decrease in the order G > A > C > T, although the C and T seems to be interchangeable. Even before BSSE, the M06-2X/6-31G(d) in the scheme of ONIOM (M06-2X/6-31G*:AM1) results in a rather weak binding and different sequence (14.8, 14.1, 16.0 and 13.8 kcal/mol for G, A, T and C.) [14] Although B3LYP-D/6-31G(d)//M06-2X/6-31G(d) done by Umadevi et al. also brings about the sequence G > A > T > C [14], the BSSE correction (9.6 kcal/mol) for cytosine–graphene complex was predicted dramatically high, while others were regular in 3.1–6.2 kcal/mol. In spite of extensive theoretical investigations into the binding between DNA bases to pristine graphene, the above discussion indicates that there is still a controversial with respect to binding strength and binding sequence. In this present study, in order to assess its performance as well as to provide consistent result for a comparison with adsorptions on defective graphene the M06-2X will be further used to optimize the adsorptions of DNA on pristine graphene and then improve the binding energy with B97-D.

During production of graphene from the thermal expansion of graphite oxide (GO), some carbon atoms are missing to form defective graphene [20]. The most common defects of graphene include mono-vacancies, multivacancies, pentagon heptagon pairs, and adatoms [21–23]. Di-vacant defective graphene is energetically favored over the mono-vacant one because of its reconstruction without dangling bond [24]. Because of carbon vacancies the defective graphene may demonstrate significant influences on the chemical and physical characteristics of graphene, for example, chemisorptions on the defect sites [25–27]. Very recently, the adsorptions of metal clusters on the mono-vacant and di-vacant defective (5-8-5 defect) graphenes were investigated [28–32]. The structural and electronic properties of the nanoparticles adsorbed on the defective graphene usually show peculiarities. The defective sites sever as anchoring points for the nanoparticles, and under-coordinated neighboring carbons further strengthen the binding of the nanoparticles to graphene layer. Catalytic reactivity of the adsorbed nanoparticles may be also enhanced. Lim found that the most stable conformation of $Pt_{13}$ on mono-vacant defective graphene has $D_{4h}$ symmetry, rather than the isolated $I_h$ symmetry, and the $Pt_{13}$ donates electron to the defective graphene and the adsorbed $O_2$ [29]. The binding of $Pt_4$ to mono-vacant graphene was 3–4 times higher than to pristine graphene.[32] A variety of gas molecules ($O_2$, CO, $N_2$, $B_2$, $H_2O$) can be chemically adsorbed on the di-vacancy defective graphene, with a magnitude of 3–13 eV binding energy [3]. The DFT predicted chemisorption of $H_2S$ on the mono-vacancy defective graphene by forming weak covalent bond (1.55 eV) [24]. However, in spite of many publications for the adsorptions of DNA nucleobases on pristine graphene as described above, to the best of our knowledge the adsorption of the defective graphene with DNA nucleobases has not been reported. Obviously, it is important to reveal the binding behavior (covalent or non-covalent) of the defective graphene with DNA nucleobases in biomedical science because the defect site of graphene could give rise to a local electronic structure change around it [33]. In the present work M06-2X and B97-D were employed to study the interaction of DNA nucleobases with mono- and di-vacant defective graphene.

## 2. Computational methods

Accurate description for noncovalent weak interaction systems like the π-stacked systems is still a challenge for density functional theory (DFT), a promising quantum mechanics method for large systems, although considerable improvements have been achieved over LDA and such conventional hybrid DFT as B3LYP in the recent years [34,35]. Recently, the novel hybrid meta-GGA functional, M06-2X, developed by Truhlar et al. [33], provides relatively reasonable results for π···π stacking systems [36]. Therefore, in this paper the geometric parameters of all nucleobase-graphene adsorption complexes are fully optimized in gas phase at M06-2X/6-31G(d) level. To obtain accurate binding energy, the bigger basis set of 6-311++G(d,p) was employed to refine the stationary point energy at both M06-2X and B97-D levels of theory with BSSE correction. Based on the suggestion of Antony and Grimme [10], the pristine graphene is modeled with $C_{72}H_{24}$, which is also compared with $C_{78}H_{24}$, $C_{86}H_{26}$, and $C_{106}H_{28}$. The defective graphenes are modeled with $C_{71}H_{24}$ for mono-vacancy and $C_{70}H_{24}$ for di-vacancy. All calculations were done using the Gaussian09 version B01 [37].

## 3. Results and discussion

### 3.1. Adsorptions of DNA nucleobases on pristine graphene

The structures of the adsorption complexes of DNA nucleobases on pristine graphene are shown in Fig. 1. The graphene sheet is modeled by $C_{72}H_{24}$, larger than the suggested minimum carbon cluster of $C_{54}$ for graphene [10]. $C_{72}H_{24}$ keeps planar and basically parallel to the rings of nucleobases. Table 1 lists the distances between graphene and the nucleobase plane for the adsorption complexes optimized at the M06-2x/6-31G(d) level. For all of the four nucleobases, the distances from the graphene to the hexagon rings are in the range of 3.103–3.137 Å, and those to the pentagon rings of adenine and guanine are 3.156 and 3.163 Å, respectively. However, the electronegative O atom is closer to the graphene with vertical distances of 2.964, 2.943, and 2.968 Å for $C_{72}H_{24}$–guanine, $C_{72}H_{24}$–thymine, and $C_{72}H_{24}$–cytosine, respectively. There may be a stronger interaction of nucleobase oxygen with the graphene plane (C═O···π) than the rings of nucleobases (π···π). Although the distances of the N atoms of $NH_2$ group from graphene are nearly identical to those of hexagon rings of nucleobases, the H atoms of the $NH_2$ group have shorter distances of 2.864, 2.606, and 2.900 Å for $C_{72}H_{24}$–adenine, $C_{72}H_{24}$–guanine, and $C_{72}H_{24}$–cytosine, respectively. For the methyl group of connected in thymine there are the distances of 3.253 and 2.580 Å from the C atom and one of the H atoms, respectively, to graphene. Because of the short distances of both amine and methyl groups with graphene, there is also weak interaction of the H atom of amino (N—H···π) or methyl group (C—H···π) with graphene.

Table 2 lists the binding energies of nucleobases with graphene together with reference data. With the $C_{72}H_{24}$ model of graphene, the binding energies at the M06-2X/6-31G(d) level are 20.2, 16.6, 15.8, and 15.6 kcal/mol for G, A, T, and C, respectively. The predicted binding is much stronger than that with ONIOM (M06-2X/6-31G*:AM1) (14.8, 14.1, 16.0, and 13.8 kcal/mol for G, A, T, and C) [14], and also shows a different sequence. The basis set 6-311++G(d,p) including diffuse and polarization of H increases the binding energies by 3.0–4.0 kcal/mol; yet the BSSE decreases the binding energies by 4.5–6.0 kcal/mol. As a result, the binding energies of G, A, T and C with $C_{72}H_{24}$ at M06-2X/6-311++G(d,p)//M06-2X/6-31G(d) level are 18.2, 14.7, 14.2, and 14.1 kcal/mol, respectively, which agree very well with the

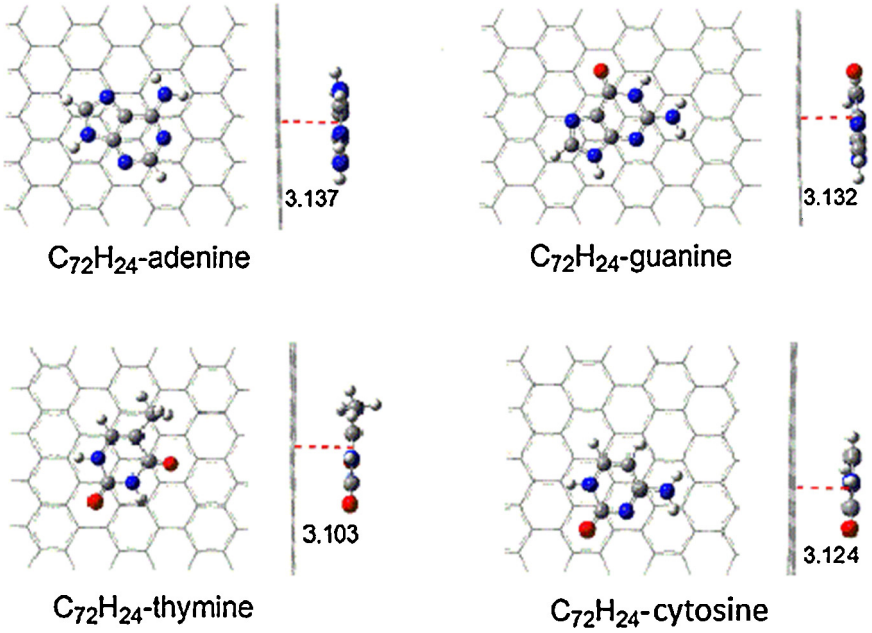


**Fig. 1.** Top and side views for the configurations of $C_{72}H_{24}$–nucleobase complexes (distances/Å).

**Table 1**
Distances (Å) between pristine graphene and nucleobases in the binding complexes optimized at the M06-2X/6-31G(d) level.

| Distance | Hexagon | Pentagon | O | $NH_2$ | $CH_3$ | | |
|---|---|---|---|---|---|---|---|
| | | | | N | H | C | H |
| $C_{72}H_{24}$–adenine | 3.137 | 3.156 | | 3.126 | 2.864 | | |
| $C_{72}H_{24}$–guanine | 3.132 | 3.163 | 2.964 | 3.129 | 2.606 | | |
| $C_{72}H_{24}$–thymine | 3.103 | | 2.943 | | | 3.253 | 2.580 |
| $C_{72}H_{24}$–cytsine | 3.124 | | 2.968 | 3.124 | 2.900 | | |

results from vdW-HF/6-31G**[11] and B3LYP-D/6-31G*//(M06-2X/6-31G*:AM1),[14] yet they are still less than the theoretical values of MP2, B2PLYP-D and wB97XD [9,10,16]. Similar to the adsorption of DNA bases on $C_{60}$ derivatives and single-walled carbon nanotubes [36,38,39], the M06-2X again is insufficient for the noncovalent interaction systems. It is known that the dispersion energy plays an important role in physisorption. For the long distance interaction between nucleobase and graphene we thus refined the binding energies with the dispersion corrected DFT, B97-D/6-311++G(d,p) for the geometries optimized with the M06-2X/6-31G(d). Table 2 shows that the binding energies at B97-D/6-311++G(d,p)//M06-2X/6-31G(d) for G, A, T and C are 27.0, 23.3, 20.8, and 19.9 kcal/mol, while they lessen to 21.6, 18.4, 16.3, and 15.8 kcal/mol, respectively with the BSSE correction. As compared with those of M06-2X/6-311++G(d,p), the binding energy increases by 3.4, 3.7, 2.1 and 1.7 kcal/mol for G, A, T and C, respectively, indicating that the dispersion energies of the adenine and guanine are larger than the thymine and cytosine because of the larger molecular sizes of G and A than those of T and C. Obviously, these binding energies are 2–5 kcal/mol

**Table 2**
Binding energies (kcal/mol) of DNA nucleobases on nano graphene ($C_{72}H_{24}$, $C_{78}H_{24}$, $C_{86}H_{26}$, $C_{106}H_{28}$) at the M06-2x and B97-D levels. The data in Basis sets, A:6-31G(d); B: 6-311++G(d,p); C:6-31G(d,p).

| | M06-2X/A | M06-2X/B// M06-2X/A | B97-D/B// M06-2X/A | MP2/B[a] | B97D/ TZV(2d,2p)[b] | vdW-HF/ C[c] | LDA[d] | vdW-DF[e] | B3LYP-D/ A//(M06-2X/A:AM1)[f] | wB97XD/ C[g] |
|---|---|---|---|---|---|---|---|---|---|---|
| $C_{72}H_{24}$–adenine | (16.6) | 14.7 (20.1) | 18.4 (23.3) | 21.7 | 20.2 | 14.8 | 14.1 | 16.4 | 15.0 | 20.3 |
| $C_{78}H_{24}$–adenine | (16.4) | 14.7 (20.2) | 18.9 (23.9) | | | | | | | |
| $C_{86}H_{26}$–adenine | (16.4) | 14.5 (20.0) | 18.4 (23.4) | | | | | | | |
| $C_{106}H_{28}$–adenine | (16.2) | 14.6 (20.0) | 19.0 (23.9) | | | | | | | |
| $C_{72}H_{24}$–guanine | (20.2) | 18.2 (24.2) | 21.6 (27.0) | 24.6 | 24.2 | 15.1 | 11.3 | | 17.5 | 22.5 |
| $C_{72}H_{24}$–thymine | (15.8) | 14.2 (19.1) | 16.3 (20.8) | 21.4 | 19.0 | 14.8 | 11.3 | | 14.3 | 18.4 |
| $C_{72}H_{24}$–cytsine | (15.6) | 14.1 (18.6) | 15.8 (19.9) | 18.4 | 18.5 | 7.9 | 11.3[a] 9.0[d] | | 13.3 | 18.9 |

[a] Ref. [9].
[b] Ref. [10].
[c] Ref. [11].
[d] Ref. [12].
[e] Ref. [13].
[f] Ref. [14].
[g] Ref. [16].

higher than the results from B3LYP-D/6-31G*//ONIOM(M06-2X/6-31G*:AM1),[14] and only 1–2 kclal/mol less than the ones of B2PLYP-D/TVZ(2df,2pd) [10]. It is essential that the present binding order (G > A > T > C) at the three levels agrees with that from the high levels such as MP2/6-311++G**[9], and B2PLYP-D/TVZ(2df,2pd) [10], yet for T and C opposite to the most recent result from wB97XD/6-31G** [16]. In order to assess the validity of the graphene size, we extended the adsorption of adenine on other three larger graphene models, $C_{78}H_{24}$, $C_{86}H_{26}$, and $C_{106}H_{28}$ as shown in Table 2. Compared with the binding energy for $C_{72}H_{24}$, the maximum deviations are only 0.4 and 0.6 kcal/mol at the M06-2X/6-31G* and B97-D/6-311++G** levels, respectively; they are excellently consistent at the M06-2X/6-311++G** level. This shows that $C_{72}H_{24}$ can well represent graphene adsorbing nucleobases in this study.

Fig. 2 displays the highest occupied frontier molecular orbitals of the $C_{72}H_{24}$–guanine complex, as an example to illustrate the interaction between nucleobases and graphene. There is almost no orbital component from guanine in HOMO, rather small contribution to HOMO-1 and HOMO-5. It is apparent that there is not much contribution of these molecular orbitals to the combination of guanine and graphene. In contrast, HOMO-2, -3 and -4 exhibit the orbital interaction between guanine and graphene. The orbital overlap of HOMO-2, -3 and -4 mainly takes place through π–π type in the hexagon and pentagon of guanine with graphene, while the p(O)-π and p(N)-π overlaps appear in HOMO-2 and HOMO-4. However, these π–π, $p_O$–π and $p_{NH}$–π interactions are quite weak because of the long distance of ~3 Å. In fact, the adsorption energy primarily comes from dispersion interaction aside from the orbital interaction, as mentioned in the above section.

In order to analyze and visualize the noncovalent interactions in these systems, an approach developed by Yang et al. was adopted [40]. In this approach, the reduced density gradient, defined as $RDG = 1/(2(3\pi^2)^{1/3})|\nabla\rho|/\rho^{4/3}$, together with electron density ($\rho$), were used to distinguish the covalent bonding and noncovalent interactions. In order to identify the noncovalent interaction, the sign of the second largest Eigenvalue ($\lambda_2$) of the electron-density Hessian was utilized as a tool to distinguish bonded ($\lambda_2 < 0$) from nonbonded ($\lambda_2 > 0$) [40]. The gradient isosurfaces are colored according to the corresponding values of sign($\lambda_2$)$\rho$. Large negative values of sign($\lambda_2$)$\rho$ are indicative of attractive interactions (such as dipole–dipole or hydrogen bonding); while if sign($\lambda_2$)$\rho$ is large and positive, the interaction is nonbonding [40]. Values near zero indicate very weak, Van der Waals interactions. The gradient isosurfaces provide a visualization of noncovalent interaction as broad regions of real space, rather than simple pairwise contacts between atoms. The functions such as RDG and sign($\lambda_2$)$\rho$ were calculated with Multiwfn software [41]. The gradient isosurface was plotted with VMD [42]. Fig. 3 shows the plot of reduced density gradient (RDG) isosurface of guanine-graphene complex. The isosurface in green color represents the Van de Waals interaction corresponding to the all atoms of guanine molecule with graphene. Especially, the groups of $NH_2$ and O have slightly stronger vdW interaction through respective N—H···π and C═O···π. The binding energy of guanine with graphene thus originates from both orbital interaction and vdW interaction.

### 3.2. Adsorptions of DNA nucleobases on mono-vacant graphene

The mono-vacant defective graphene model, $C_{71}H_{24}$, is derived from the pristine graphene model, $C_{72}H_{24}$, by removing a carbon atom, as shown in Fig. 4. The geometries of $C_{71}H_{24}$ were optimized for four electronic states. For the closed shell singlet state (a) the configuration has two pentagon rings and the C1 atom is of near tetrahedral structure, a significant distortion of the graphene plane. The open shell singlet configuration (not shown) has one pentagon ring and a carbene-like atom, C1, and much less stable than the closed shell by 32.0 kcal/mol. The C2—C3 bond length of the triplet

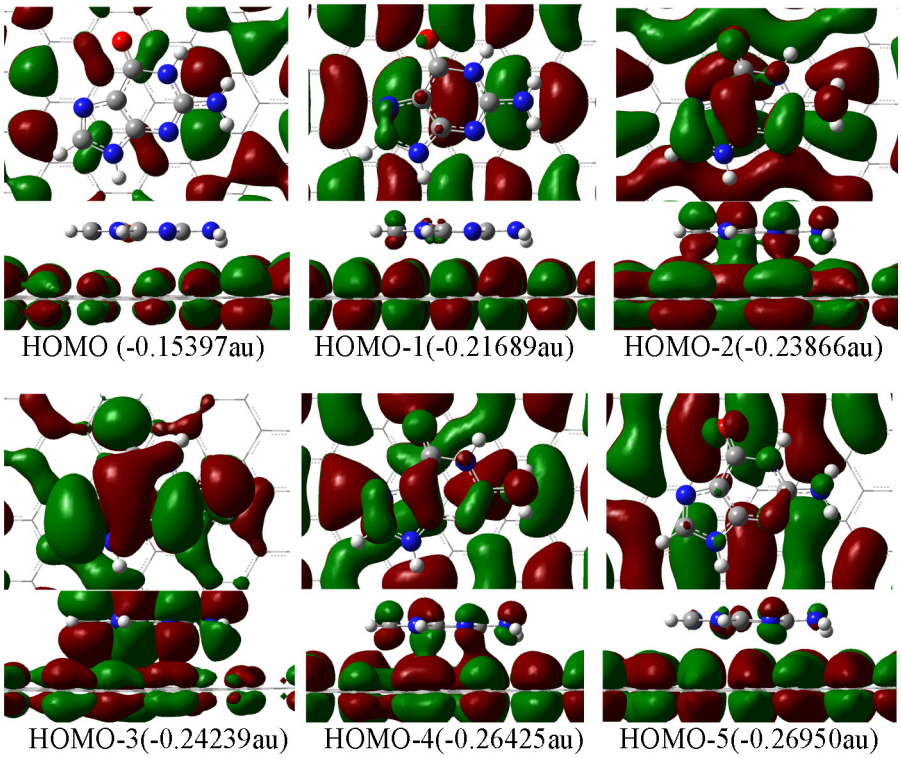


**Fig. 2.** Top and side views of orbital iso-surfaces (0.002 a.u.) of graphene–guanine complex from HOMO to HOMO-5. Orbital energies are in parantheses. Orbital interaction occurs only in HOMO-2, HOMO-3 and HOMO-4.

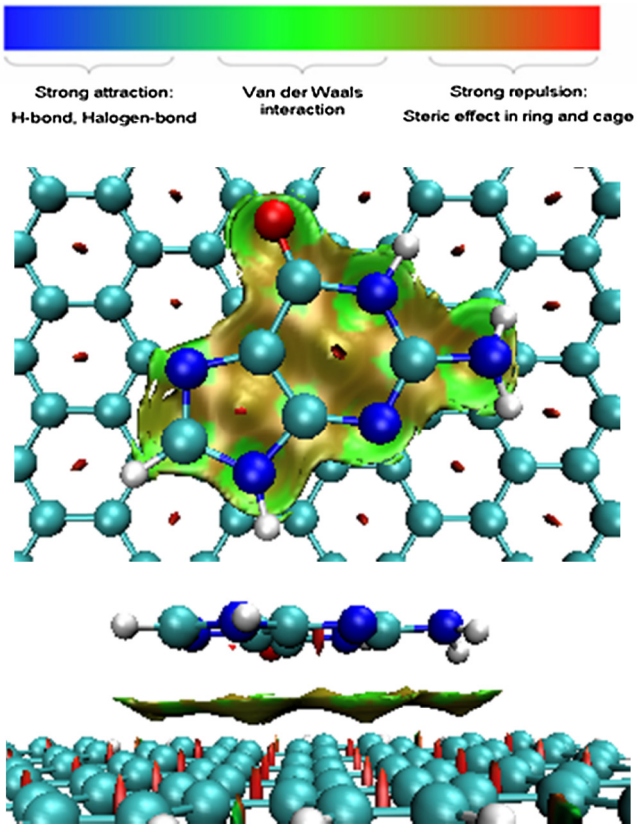


**Fig. 3.** Top (top) and side (bottom) views of sign($\lambda_2$)$\rho$ isosurface of graphene–guanine complex. Green and yellow denote vdW interaction between guanine and graphene through π···π, C═O···π, and N/C—H···π. (For interpretation of the references to color in this figure legend, the reader is referred to the web version of the article.)

configuration in Fig 4b is 1.715 Å and the atomic distances of C1–C2 and C1—C3 are 2.650 Å, and the triplet is more stable than the closed and open shell singlet states by 8.1 and 40.1 kcal/mol, respectively. In addition, the quintet configuration of $C_{71}H_{24}$ has similar structure to triplet, in which the bond length of C2—C3 is 1.748 Å and the atomic distances of C1—C2 and C1—C3 are 2.635 Å; however, it is less stable than the triplet one by 1.5 kcal/mol. Thus, the ground state of $C_{71}H_{24}$ exhibits biradical character and the triplet state was thus used to investigate the adsorption of DNA nucleobases on graphene.

Fig. 5 shows the structures of the adsorption complexes of nucleobases on mono-vacant defective graphene of the triplet $C_{71}H_{24}$.

**Table 3**
Binding energies (kcal/mol) of DNA nucleobases on mono-vacant defective graphene ($C_{71}H_{24}$) at the M06-2X and B97-D levels. The data in the parenthesis refer to those without BSSE. Basis sets, A:6-31G(d); B:6-311++G(d,p).

| | M06-2X/A | M06-2X/B//M06-2X/A | B97-D/B//M06-2X/A |
|---|---|---|---|
| Adenine | | | |
| $C_{71}H_{24}$–ade-a | **16.2** | **14.2 (19.2)** | **17.5 (22.2)** |
| $C_{105}H_{28}$–ade-a | **16.5** | **14.3 (19.5)** | **18.0 (22.8)** |
| $C_{71}H_{24}$–ade-b | 15.4 | 13.4 (18.4) | 16.3 (21.0) |
| $C_{71}H_{24}$–ade-c | 15.3 | 13.5 (18.2) | 16.4 (20.8) |
| Guanine | | | |
| $C_{71}H_{24}$–gua-a | 18.7 | 16.6 (22.3) | 18.9 (24.2) |
| $C_{71}H_{24}$–gua-b | 18.4 | 16.4 (22.0) | 17.1 (22.3) |
| $C_{71}H_{24}$–gua-c | **19.2** | **17.0 (22.5)** | **19.5 (24.6)** |
| $C_{71}H_{24}$–gua-d | 17.8 | 15.7 (21.0) | 18.8 (23.7) |
| Thymine | | | |
| $C_{71}H_{24}$–thy-a | 15.2 | 13.7 (18.3) | 14.4 (18.6) |
| $C_{71}H_{24}$–thy-b | 16.7 | 15.3 (19.8) | 17.3 (21.5) |
| $C_{71}H_{24}$–thy-c | **17.3** | **15.8 (20.2)** | **18.3 (22.3)** |
| Cytosine | | | |
| $C_{71}H_{24}$-cyt-a | 14.2 | 12.4 (16.9) | 13.2 (17.3) |
| $C_{71}H_{24}$-cyt-b | **16.0** | **14.5 (18.9)** | **16.1 (20.2)** |
| $C_{71}H_{24}$-cyt-c | 15.3 | 13.8 (18.0) | 15.8 (19.6) |

The bold values refer to the predicted strongest binding.

Because of the missing carbon atom in the graphene plane, the interaction between graphene and nucleobase causes the graphene plane a slightly bending. The different position of the hexagonal ring of nucleobase over the defective graphene leads to a number of adsorption complexes. For $C_{71}H_{24}$–adenine complex three configurations are located at the M062x/6-31G* level of theory. The adsorption energies are summarized in Table 3. Among the three complexes $C_{71}H_{24}$–ade-a has the highest adsorption energy of 16.2 kcal/mol at the M062x/6-31G*, and is more stable than $C_{71}H_{24}$–ade-b and $C_{71}H_{24}$–ade-c by 0.8 and 0.9 kcal/mol, respectively. The distances of $C_1$—$C_2$ and $C_1$—$C_3$ of $C_{71}H_{24}$ in $C_{71}H_{24}$–ade-a only slightly stretch to 2.661 Å from 2.650 Å of the free $C_{71}H_{24}$, while the $C_2$—$C_3$ compresses a little to 1.709 Å from 1.715 Å. The shortest atomic distance in $C_{71}H_{24}$–ade-a is ~3.180 Å. With BSSE correction the adsorption energies for $C_{71}H_{24}$–ade-a, -b and -c are 14.2, 13.4, and 13.5 kcal/mol, respectively, at the M062x/6-311++G(d, p) level; while they respectively increase to 17.5, 16.3, and 16.4 kcal/mol at the B97D/6-311++G(d, p) level. In addition, the complex of the bigger graphene model with adenine, $C_{105}H_{28}$–ade-a, was re-optimized to compare with $C_{71}H_{24}$–ade-a, and the adsorption energy is just slightly higher by 0.1 and 0.5 kcal/mol at the M062x and B97D levels, respectively.

For the $C_{71}H_{24}$-guanine system, four adsorption complexes were located at the M06-2X/6-31G* level, as shown in Fig. 5.

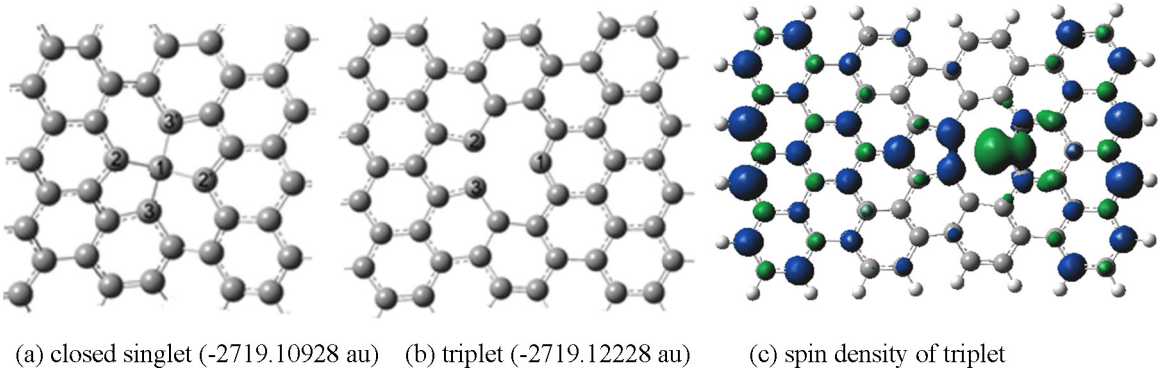


**Fig. 4.** Structures of $C_{71}H_{24}$ at singlet and triplet at M06-2x/6-31G*, and spin density for the triplet. (a) $C_1$—$C_2$ = 1.5946 Å, $C_1$–$C_3$ = 1.6141 Å, $\angle C_2C_1C_{2'}$ = 138.3°, $\angle C_3C_1C_{3'}$ = 138.1° (b) triplet state: $C_1$–$C_2$ = 2.6502 Å, $C_1$—$C_3$ = 2.6502 Å, $C_2$—$C_3$ = 1.7153 Å. (quintet: $C_1$—$C_2$ = 2.6344 Å, $C_1$—$C_3$ = 2.6345 Å, $C_2$—$C_3$ = 1.7484 Å) (c) Spin density (isosurface = 0.004 a.u.).

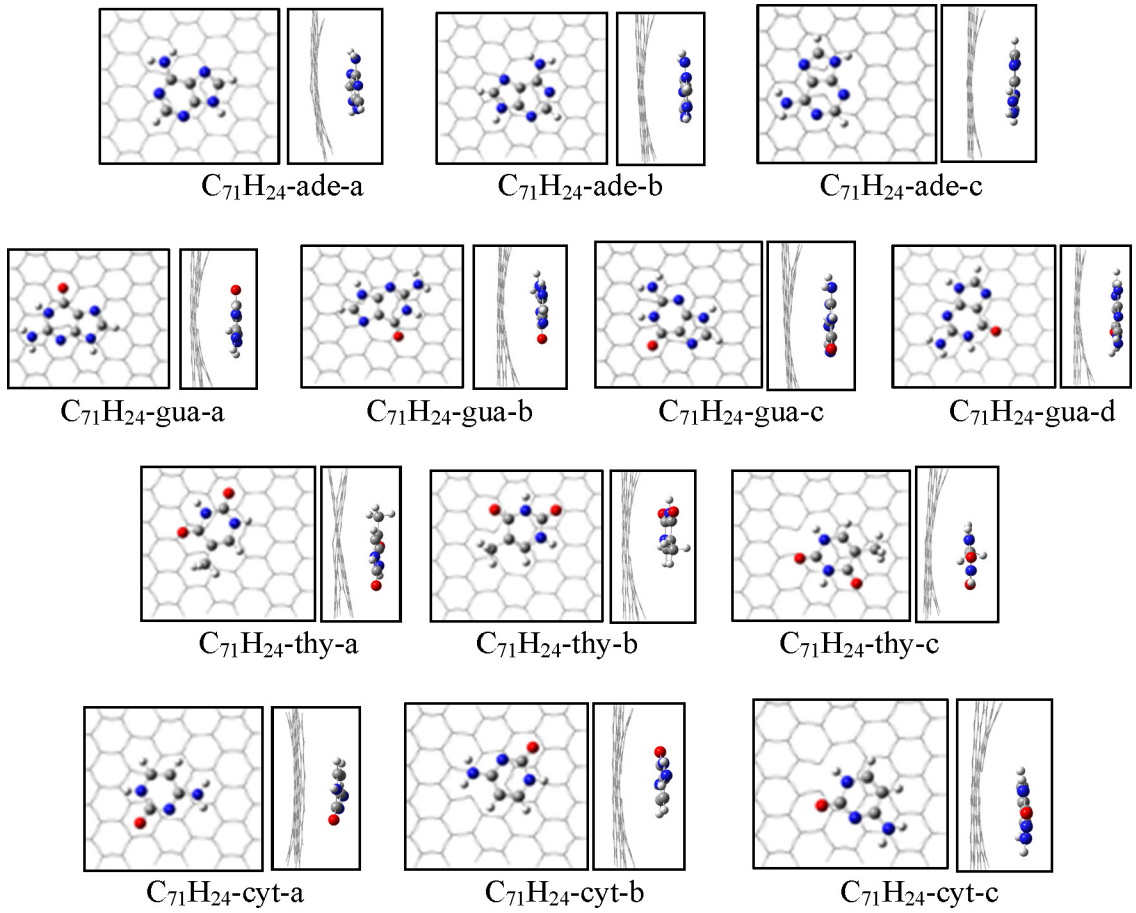


**Fig. 5.** Top and side views for the adsorption complexes of nucleobases on monovacancy defective graphene ($C_{71}H_{24}$).

Among the four adsorption complexes the most stable complex is $C_{71}H_{24}$–gua-c, with the adsorption energies of 17.0 and 19.5 kcal/mol at the M06-2X/6-311++G(d, p) and B97D/6-311++G(d, p) levels, respectively. Similar to the adsorptions on pristine graphene, guanine more strongly binds to the defective graphene than adenine does.

For the $C_{71}H_{24}$–thymine system, $C_{71}H_{24}$–thy-c has the highest adsorption energy among three adsorption configurations. With BSSE correction at 6-311++G(d,p), the adsorption energy of $C_{71}H_{24}$–thy-c is 15.8 kcal/mol at M06-2X level, 2.1 and 0.5 kcal/mol greater than $C_{71}H_{24}$–thy-a and $C_{71}H_{24}$–thy-b, respectively; while at the B97D level the adsorption energy of $C_{71}H_{24}$–thy-c is 18.3 kcal/mol, greater than $C_{71}H_{24}$–thy-a and $C_{71}H_{24}$–thy-b by 3.9 and 1.0 kcal/mol, respectively. Although cytosine has the same hexagon ring as thymine, the different substitutes may lead to the adsorption energy of $C_{71}H_{24}$–cytosine less than that of $C_{71}H_{24}$–thymine. The most stable complex among three $C_{71}H_{24}$–cytsine configurations is $C_{71}H_{24}$-cyt-b with the binding energies of 14.5 and 16.1 kcal/mol at the M06-2X and B97D/6-311++G(d,p) levels, respectively. The adsorption energy of $C_{71}H_{24}$-cyt-b is 2.1 and 2.9 kcal/mol higher than those of $C_{71}H_{24}$-cyt-a at M06-2X and B97D levels, respectively; while it is only 0.7 and 0.3 kcal/mol, respectively greater than the ones of $C_{71}H_{24}$-cyt-c.

Although the mono-vacant defective graphene was shown to chemically bind to various molecules and metal cluster through the defective sites, dramatically stronger than to pristine graphene [3,24,28,29,32], the above discussions reveal that the DNA bases adsorbs on the mono-vacant graphene through noncovalent interaction with the shortest atomic distances of approximately 3.1–3.2 Å. The spin density in Fig. 6 for $C_{71}H_{24}$-gau-c dominantly locates over the mono-vacant graphene, also indicating the noncovalent interaction between the DNA base with the defective graphene. On the contrary, the spin density of the complex of $Pt_4$ and mono-vacant graphene considerably delocalizes over the Pt (65%) and graphene (35%) clusters, which can be to attributed to the similar SOMOs of $Pt_4$ and $C_{103}H_{28}$ clusters (−0.185 vs −0.162au) and thus significant orbital overlap leads to strong binding [32]. The difference between the HOMO of guanine and the SOMO of $C_{71}H_{24}$ (0.258 vs 0.193 a.u.) is relatively high, and the minor orbital overlap excludes the covalent interaction and Van der Waals interaction is still the dominant interaction between DNA bases and the defective graphene.

The noncovalent Van der Waals interaction was illustrated in Fig. 7 through the color filled sign($\lambda 2$)$\rho$ at the isosurface of RDG = 0.5, where the green and yellow areas show the vdW interaction between guanine and the mono-vacant graphene through π···π, C═O···π, and N/C—H···π. A comparison among the most stable complexes for DNA bases indicates that the adsorption energies decrease by the sequence of G (19.5 kcal/mol) > T (18.3) > A (17.5–18.0) > C (16.1), which is different from the adsorptions on pristine graphene $C_{72}H_{24}$ (G > A > T > C: 21.6, 18.4–19.0, 16.3, 15.8 kcal/mol) by switching the sequence of adenine and thymine. In addition, the adsorption energies of adenine and guanine on the defective graphene $C_{71}H_{24}$ are approximately 1–2 kcal/mol less than on the pristine graphene $C_{72}H_{24}$, while $C_{71}H_{24}$–thymine and $C_{71}H_{24}$–cytosine are 2.0 and 0.3 kcal/mol greater than those of $C_{72}H_{24}$–thymine and $C_{72}H_{24}$–cytosine, respectively. This difference may be related to the orbital overlaps and electrostatic interactions between the graphene and nucleobases. The frontier orbitals of nucleobases with $C_{71}H_{24}$ and $C_{72}H_{24}$ are displayed in

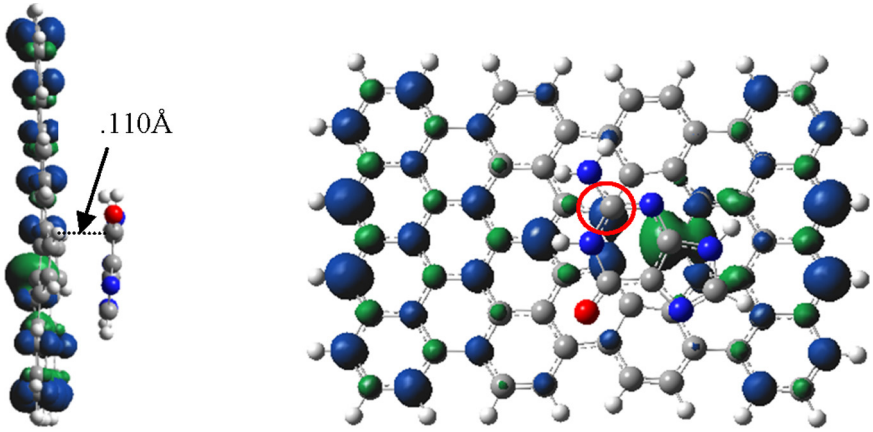


**Fig. 6.** the side (left) and top (right) views for the spin density of $C_{71}H_{24}$–gua-c (0.004 a.u.).

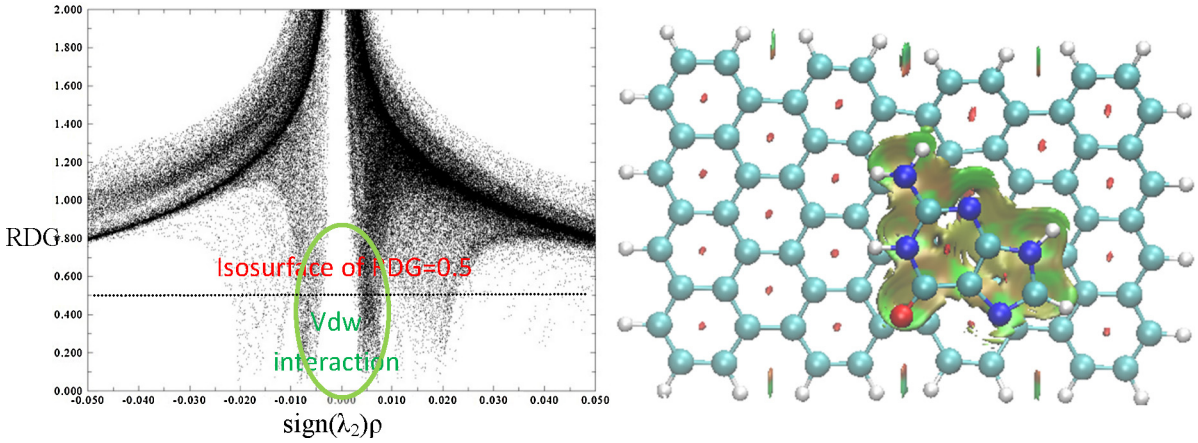


**Fig. 7.** The scatter plot of RDG vs sign(λ2)$\rho$ (left), and color filled sign(λ2)$\rho$ at the isosurface of RDG = 0.5. It has the same color code as in Fig. 3. Green and yellow areas show the vdW interaction between guanine and the mono-vacant graphene through π···π, C = O···π, and N/C-H···π.(For interpretation of the references to color in this figure legend, the reader is referred to the web version of the article.)

Supplementary Information document. For both $C_{72}H_{24}$–ade and $C_{72}H_{24}$–gua, their HOMO-2, -3 and HOMO-4 have significant orbital overlaps, but the HOMOs of both $C_{71}H_{24}$–ade and $C_{71}H_{24}$–gua have much smaller orbital overlaps because of the missing carbon atom. The electrostatic attractive energies between graphene and nucleobase in $C_{72}H_{24}$–ade and $C_{72}H_{24}$–gua are also about 0.5 kcal/mol higher than those in $C_{71}H_{24}$–ade and $C_{71}H_{24}$–gua, as in Table 4. This implies that the combining strength of the defective graphene with adenine and guanine lessens slightly relative to that of the pristine graphene with adenine and guanine. On the contrary, there is no much orbital overlap between $C_{72}H_{24}$ and thymine in the investigated HOMOs of $C_{72}H_{24}$–thy, but the HOMO-5 and HOMO-7 of $C_{71}H_{24}$–thy show small orbital interaction. For both $C_{72}H_{24}$-cyt and $C_{71}H_{24}$-cyt, the HOMO-4 orbitals have small overlap between graphene and cytosine, while the other HOMOs do not present orbital interaction. Also, the electrostatic energies of both parts of $C_{72}H_{24}$–thy and $C_{72}H_{24}$-cyt are slightly less than those of $C_{71}H_{24}$–thy and $C_{71}H_{24}$-cyt, respectively, the former by 0.13 kcal/mol and the latter by 0.03 kcal/mol. This may account for the adsorption energies of $C_{72}H_{24}$–thy and $C_{72}H_{24}$-cyt smaller than those of $C_{71}H_{24}$–thy and $C_{71}H_{24}$-cyt, respectively.

**Table 4**
Electrostatic energy estimated with CHelpG charges (kcal/mol).

| | $C_{72}H_{24}$ | $C_{71}H_{24}$ | $C_{70}H_{24}$-base |
|---|---|---|---|
| Adenine | −0.940 | −0.330 | −1.681 |
| Guanine | −2.603 | −2.113 | −3.048 |
| Thymine | −1.043 | −1.171 | −1.060 |
| Cytosine | −1.784 | −1.813 | −1.564 |

### 3.3. *Adsorptions of DNA nucleobases on divacancy defective graphene*

In addition, the di-vacant graphene ($C_{70}H_{28}$) with two missing carbon atoms has also been studied. The triplet $C_{70}H_{28}$ again is the ground state with 5-8-5-ring structure, 8.9 and 10.8 kcal/mol more stable than the singlet and quintet states, respectively. Fig. 8 shows the structures of the adsorption complex of $C_{70}H_{28}$ with nucleobases at the M06-2x/6-31G* level and Table 5 lists the adsorption energies at the M06-2x and B97-D levels. The adsorption between di-vacant graphene and nucleobase seems not favorable on the twisted graphene surface and at the octagonal vacant position because of bigger vacant hole of the octagonal ring. Among the three adsorption complexes of $C_{70}H_{24}$–adenine, the least stable complex is $C_{70}H_{24}$–ade-a, in which the hexagonal ring of adenine mostly sits above the octagonal ring of $C_{70}H_{24}$ and the graphene surface is twisted, while $C_{70}H_{24}$–ade-b and $C_{70}H_{24}$–ade-c have stronger adsorption because the fragment of adenine is located on the octagonal boundary of $C_{70}H_{24}$. With BSSE correction for $C_{70}H_{24}$–ade-a, -b, and -c, the respective adsorption energies are 12.7, 14.7, and 15.9 kcal/mol at M06-2X/6-311++G**; and they increase to 16.6, 19.0, and 19.9 kcal/mol at B97-D/6-311++G**. For the case of $C_{70}H_{24}$–gua at the M06-2X/6-31G* level the adsorption

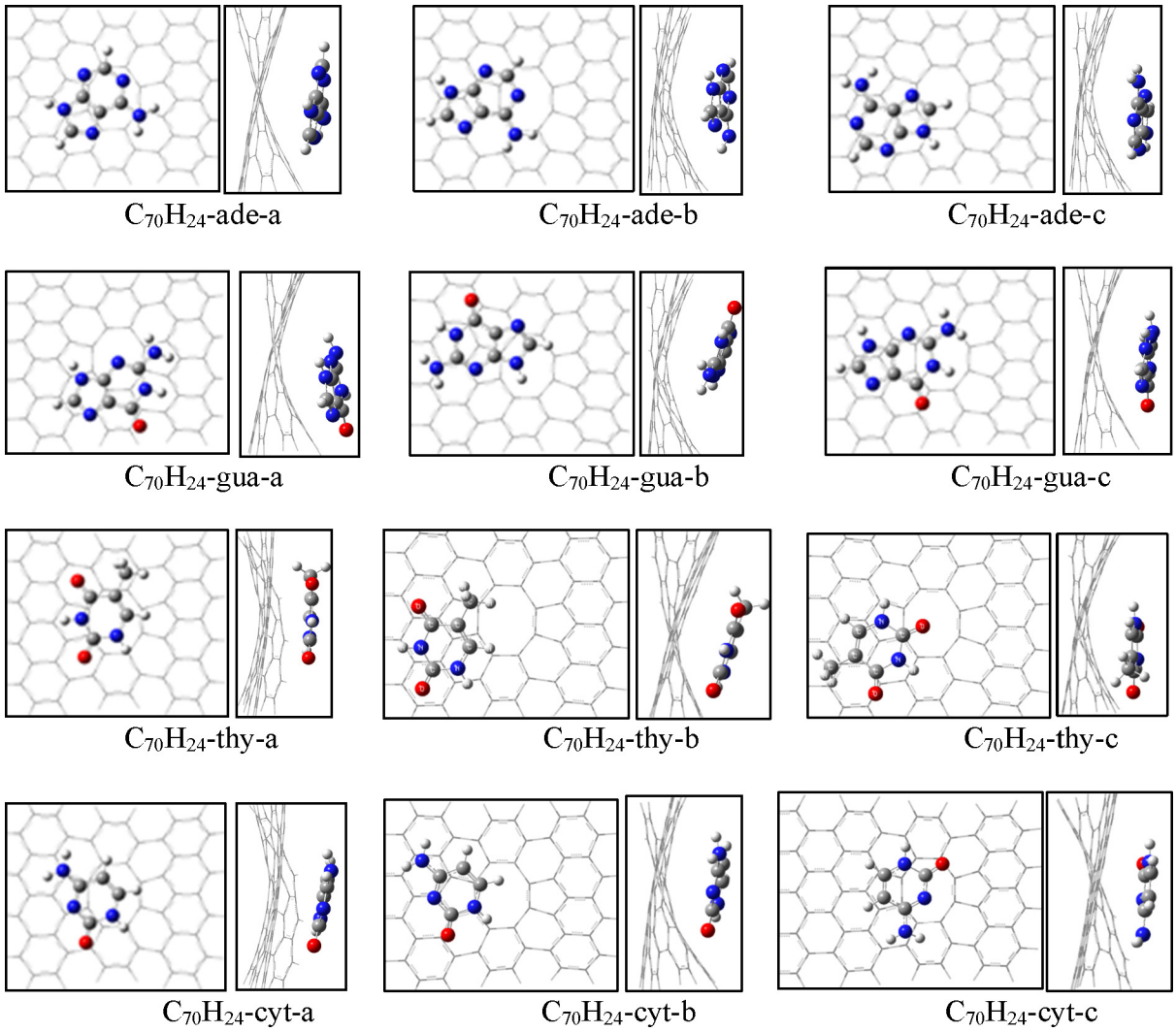


**Fig. 8.** Top and side views of the adsorption complexes of nucleobases on di-vacant defective graphene ($C_{70}H_{24}$).

**Table 5**
Binding energies (kcal/mol) of DNA nucleobases on divacancy defective graphene ($C_{70}H_{24}$) at the M06-2x and B97-D levels. Basis sets: A, 6-31G(d); B, 6-311++G(d,p). Numbers in parentheses refer to the binding energies without BSSE.

| | M062x/A | M062-2X/B//M06-2X/A | B97D/B//M06-2X/A |
|---|---|---|---|
| Adenine | | | |
| $C_{70}H_{24}$–ade-a | (15.1) | 12.7 (17.6) | 16.6 (21.2) |
| $C_{70}H_{24}$–ade-b | (16.6) | 14.7 (19.7) | 19.0 (23.6) |
| $C_{70}H_{24}$–ade-c | **(17.9)** | **15.9 (21.0)** | **19.9 (24.6)** |
| Guanine | | | |
| $C_{70}H_{24}$–gua-a | (21.8) | 19.1 (24.3) | 21.4 (26.1) |
| $C_{70}H_{24}$–gua-b | (21.0) | 19.0 (24.6) | 23.3 (28.4) |
| $C_{70}H_{24}$–gua-c | **(20.6)** | **18.0 (23.7)** | **21.5 (26.8)** |
| Thymine | | | |
| $C_{70}H_{24}$–thy-a | (15.8) | 14.1 (18.6) | 16.4 (20.5) |
| $C_{70}H_{24}$–thy-b | (16.4) | 14.5 (19.2) | 17.4 (21.7) |
| $C_{70}H_{24}$–thy-c | **(17.6)** | **16.0 (20.5)** | **18.9 (23.1)** |
| $C_{86}H_{26}$–thy-a | (15.9) | | |
| $C_{86}H_{26}$–thy-b | (15.8) | | |
| $C_{86}H_{26}$–thy-c | (18.2) | | |
| Cytosine | | | |
| $C_{70}H_{24}$–cytsine-a | (14.7) | 13.2 (17.6) | 15.3 (19.3) |
| $C_{70}H_{24}$–cytsine-b | **(15.6)** | **14.2 (18.6)** | **16.9 (21.0)** |
| $C_{70}H_{24}$–cytsine-c | (13.8) | 11.6 (16.1) | 14.8 (18.8) |

The bold values refer to the predicted strongest binding.

energy of $C_{70}H_{24}$–gua-a is the highest among three adsorption structures, while with 6-311++G** basis set the adsorption energies of $C_{70}H_{24}$–gua-a and -b are almost identical. However, at the B97-D/6-311++G** level $C_{70}H_{24}$–gua–b has the highest adsorption energy. Table 5 shows that the adsorption energies of $C_{70}H_{24}$–gua-a, -b, and -c are 19.1, 19.0, and 18.0 kcal/mol, respectively, at M06-2X/6-311++G** level, and 21.4, 23.3, and 21.5 kcal/mol at B97-D/6-311++G**, which are obviously greater than those of $C_{70}H_{24}$–ade. As for both $C_{70}H_{24}$–thy and $C_{70}H_{24}$-cyt, the most stable structures are $C_{70}H_{24}$–thy-c and $C_{70}H_{24}$-cyt-b, respectively. At the B97D + BSSE level the adsorption energy of the former is 18.9 kcal/mol and the latter is 16.9 kcal/mol. The adsorption energy of $C_{70}H_{24}$–thy is about 2.0 kcal/mol more than that of $C_{70}H_{24}$-cyt, and ~1.0 and 4.4 kcal/mol less than those of $C_{70}H_{24}$–ade-c and $C_{70}H_{24}$–gua-b, respectively. The adsorption energies of DNA bases on the di-vacant graphene descend by the sequence of G > A > T > C, which is consistent with the sequence of $C_{72}H_{24}$-nucleobases and slightly different from that of $C_{71}H_{24}$-nucleobases.

From the above discussion, although the binding for the three adsorption systems is different with respect to strength and sequence, but Van der Waals interactions are dominant for the adsorptions of DNA bases on pristine and the defective graphenes. A comparison of the adsorption energies on the pristine, mono- and di-vacant graphenes at the B97-D/6-311++G(d,p) level with

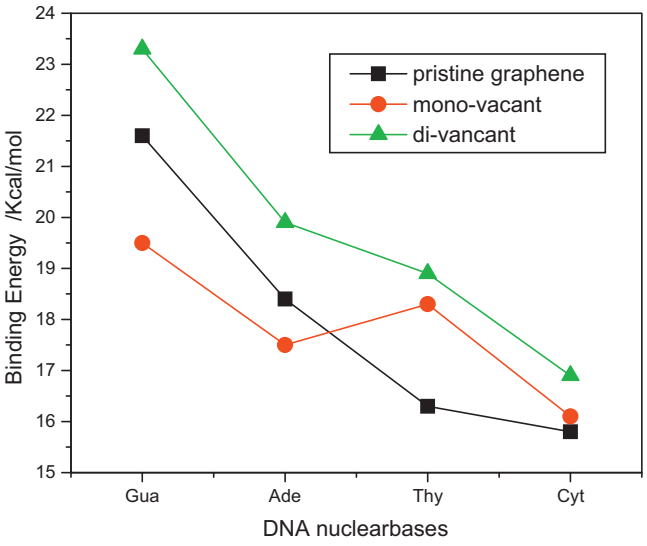


**Fig. 9.** Comparison of the binding energies of three kinds of adsorption systems. (■: pristine graphene; (● ): mono-vacant graphene; (▲ ) di-vacant graphene).

BSSE correction is shown in Fig. 9. The adsorption energies of DNA bases on the di-vacant graphene are larger than that of pristine graphene by 1.1–2.6 kcal/mol; however, for the mono-vacant defective grapheme the adsorption energies of both $C_{71}H_{24}$–gua and $C_{71}H_{24}$–ade are less than those of $C_{72}H_{24}$–gua and $C_{72}H_{24}$–ade by 2.1 and 0.9 kcal/mol, respectively, while the adsorption energy of $C_{71}H_{24}$–thy is 2.0 kcal/mol significantly larger than that of $C_{72}H_{24}$–thy and the adsorption energy of $C_{71}H_{24}$-cyt is almost equal to that of $C_{72}H_{24}$-cyt. This implies that, from pristine graphene to mono-vacancy, the binding strength decreases for guanine and adenine and increases only for thymine.

## 4. Conclusion

The adsorptions of the nucleobases G, A, C, and T on pristine, mono-vacant, and di-vacant graphenes are fully optimized at M062x/6-31G(d) level, and the adsorption energies are refined with a larger basis set of 6-311++G(d,p) at the M062x and B97D levels. Although some metal clusters and molecules tend to chemically bind to defective graphenes, it is interesting that the present investigation shows that the adsorption of DNA bases on mono- and di-vacant defective graphenes does not show much difference from that on pristine graphene, and is still dominantly driven by non-covalent interactions. At the B97D/6-311++G(d,p)//M06-2X/6-31G(d) level, the respective adsorption energies of G, A, T, and C on the pristine graphene are predicted to be 21.6, 18.4, 16.3, and 15.8 kcal/mol, and on the mono-vacant graphene they change to 19.5, 17.5, 18.3, and 16.1 kcal/mol; yet on the di-vacant graphene their binding were enhanced to 23.3, 19.9, 18.9, and 16.9 kcal/mol, respectively. This result shows that the binding strength increases from pristine graphene to di-vacant graphene for all of the four nucleobases, and to mono-vacant graphene always increase for thymine and cytosine and yet decreases for guanine and adenine. In three adsorption systems, the sequence of the adsorption strength is G > A > T > C for the pristine and di-vacant graphenes and G > T > A > C for the mono-vacant graphene.

## Acknowledgements

This work was supported by the National Institute of General Medical of the National Institute of Health (SC3GM082324), the American Recovery and Reinvestment Act (3SC3GM082324-02S1), and also in part by the Albany State University Undergraduate Research Program (Summer 2012 to Darnashley Eustache).

## References

[1] K. Geim, Status and prospects, Science 324 (2009) 1530–1534.
[2] B. Huang, Z. Li, Z. Liu, G. Zhou, S. Hao, J. Wu, et al., Adsorption of gas molecules on graphene nanoribbons and its implication for nanoscale molecule sensor, J. Phys. Chem. C. 112 (2008) 13442–13446.
[3] B. Sanyal, O. Eriksson, U. Jansson, H. Grennberg, Molecular adsorption in graphene with divacancy defects, Phys. Rev. B 79 (2009), 113409/1-/4.
[4] W. Yang, K.R. Ratinac, S.P. Ringer, P. Thordarson, J.J. Gooding, F. Braet, Carbon nanomaterials in biosensors: should you use nanotubes or graphene? Angew. Chem. Int. Ed. 49 (2010) 2114–2138.
[5] T. Nelson, B. Zhang, O.V. Prezhdo, Detection of nucleic acids with graphene nanopores: Ab initio characterization of a novel sequencing device, Nano Lett. 1 (2010) 3237–3242.
[6] K. Yang, S. Zhang, G. Zhang, X. Sun, S.-T. Lee, Z. Liu, Graphene in mice: ultrahigh in vivo tumor uptake and efficient photothermal therapy, Nano Lett. 10 (2010) 3318–3323.
[7] Y. Lin, S. Taylor, H.P. Li, K.A.S. Fernando, L.W. Qu, W. Wang, et al., Advances toward bioapplications of carbon nanotubes, J. Mater. Chem. 14 (2004) 527–541.
[8] Y. Wang., Theoretical evidence for the stronger ability of thymine to disperse SWNT than cytosine and adenine: self-stacking of DNA bases vs. Their cross stacking with SWCNT, J. Phys. Chem. C 112 (2008) 14297–14305.
[9] S. Gowtham, R.H. Scheicher, R. Ahuja, R. Pandey, S.P. Karna, Physisorption of nucleobases on graphene: density-functional calculations, Phys. Rev. B 76 (2007), 033401/1-/4.
[10] J. Antony, S. Grimme, Structures and interaction energies of stacked graphene-nucleobase complexes, Phys. Chem. Chem. Phys. 10 (2008) 2722–2729.
[11] N. Varghese, U. Mogera, A. Govindaraj, A. Das, P.K. Maiti, A.K. Sood, et al., Binding of DNA nucleobases and nucleosides with graphene, ChemPhysChem 10 (2009) 206–210.
[12] Y.-H. Zhang, K.-G. Zhou, K.-F. Xie, C.-H. Liu, H.-L. Zhang, Y. Peng, et al., First principles study of cytosine adsorption on graphene, Int. J. Nanosci. 08 (2009) 5–8.
[13] K. Berland, S.D. Chakarova-Käck, V.R. Cooper, D.C. Langreth, E. Schröder, A Van derWaals density functional study of adenine on graphene: single-molecular adsorption and overlayer binding, J. Phys.: Condens. Matter 23 (2011), 135001/1-/8.
[14] D. Umadevi, G.N. Sastry, Quantum mechanical study of physisorption of nucleobases on carbon materials: graphene versus carbon nanotubes, J. Phys. Chem. Lett. 2 (2011) 1572–1576.
[15] B. Song, G. Cuniberti, S. Sanvito, H. Fang, Nucleobase adsorbed at graphene devices: Enhance bio-sensorics, Appl. Phys. Lett. 100 (2012), 063101/1-4.
[16] S. Panigrahi, A. Bhattachary, S. Banerjee, D. Bhattacharyya, Interaction of nucleobases with wrinkled graphene surface: dispersion corrected DFT and AFM studies, J. Phys. Chem. C. 116 (2012) 4374–4379.
[17] M. Dion, H. Rydberg, E. Schroder, D.C. Langreth, B.I. Lundqvist, Van der Waals density functional for general geometries, Phys. Rev. Lett. 92 (2004) 246401.
[18] M. Dion, H. Rydberg, E. Schroder, D.C. Langreth, B.I. Lundqvist, Erratum: Van der Waals Density functional for general geometries, Phys. Rev. Lett. 95 (2005) 109902.
[19] T. Thonhauser, V.R. Cooper, S. Li, A. Puzder, P. Hyldgaard, D.C. Langreth, Van der Waals density functional: Self-consistent potential and the nature of the van der Waals bond, Phys. Rev. B. 76 (2007) 125112.
[20] K.N. Kudin, B. Ozbas, H.C. Schniepp, R.K. Prud'homme, I.A. Aksay, R. Car, Raman spectra of graphite oxide and functionalized graphene sheets, Nano Lett. 8 (2008) 36–41.
[21] A. Hashimoto, K. Suenaga, A. Gloter, K. Urita, S. Iijima, Direct evidence for atomic defects in graphene layers, Nature 430 (2004) 870–873.
[22] H.C. Schniepp, J.L. Li, M.J. McAllister, H. Sai, M. Herrera-Alonso, D.H. Adamson, et al., Functionalized single graphene sheets derived from splitting graphite oxide, J. Phys. Chem. B. 110 (2006) 8535–8539.
[23] G.-D. Lee, C.Z. Wang, E. Yoon, N.-M. Hwang, D.-Y. Kim, K.M. Ho, Diffusion, coalescence, and reconstruction of vacancy defects in graphene layers, Phys. Rev. Lett. 95 (2005) 205501.
[24] D. Borisova, V. Antonov, A. Proykova, Hydrogen sulfide adsorption on a defective graphene, Int. J. Quant. Chem. (2012) 1–6.
[25] D.W. Boukhvalov, M.I. Katsnelson, Chemical functionalization of graphene with defects, Nano Lett. 8 (2008) 4373–4379.
[26] H.L. Wang, J.T. Robinson, G. Diankov, H.J. Dai, Nanocrystal growth on graphene with various degrees of oxidation, J. Am. Chem. Soc. 132 (2010) 3270–3271.
[27] H. Terrones, R. Lv, M. Terrones, M.S. Dresselhaus, The role of defects and doping in 2D graphene sheets and 1D nanoribbons, Rep. Prog. Phys. 75 (2012) 062501.
[28] D.-H. Lim, A.S. Negreira, J. Wilcox, DFT studies on the interaction of defective graphene-supported Fe and Al nanoparticles, J. Phys. Chem. C 115 (2011) 8961–8970.
[29] D.-H. Lim, J. Wilcox, DFT-based study on oxygen adsorption on defective graphene-supported Pt nanoparticles, J. Phys. Chem. C 115 (2011) 22742–22747.

[30] R. Kou, Y. Shao, D. Mei, Z. Nie, D. Wang, C. Wang, et al., Stabilization of electrocatalytic metal nanoparticles at metal-metal oxide-graphene triple Junction points, J. Am. Chem. Soc. 133 (2011) 2541–2547.
[31] G. Kim, S.-H. Jhi, Carbon monoxide-tolerant platinum nanoparticle catalysts on defect-engineered graphene, ACS Nano. 5 (2011) 805–810.
[32] Y. Wang, Z. Xu, Adsortion and oxidation of ethanol on Pt-particles supported by defective graphene, 245th ACS National Meeting, New Orleans, 2013.
[33] Y. Zhao, N.E. Schultz, G.D. Truhlar, Design of density functionals by combining the method of constraint satisfaction with parametrization for thermochemistry, thermochemical kinetics, and noncovalent interactions, J. Chem. Theory Comput. 2 (2006) 364–382.
[34] X. Xu, W.A. Goddard III, The X3LYP extended density functional for accurate descriptions of nonbond interactions, spin states, and thermochemical properties, Proc. Natl. Acad. Sci. U.S.A. 101 (2004) 2673–2677.
[35] H. Tachikawa, H. Kawabata, Electronic states of defect sites of graphene model compounds: A DFT and direct molecular orbital–molecular dynamics study, J. Phys. Chem. C. 113 (2009) 7603–7609.
[36] W. Sun, Y. Bu, Y. Wang, On the binding strength sequence for nucleic acid bases and C60 with density functional and dispersion-corrected density functional theories: whether C60 could protect nucleic acid bases from radiation-induced damage, J. Phys. Chem. C. 115 (2011) 3220–3228.
[37] M.J. Frisch, G.W. Trucks, H.B. Schlegel, G.E. Scuseria, M.A. Robb, J.R. Cheeseman, et al., Gaussian 09, Revision A.02, Gaussian, Inc., Pittsburgh PA, 2009.
[38] W. Sun, Y. Bu, Y. Wang, Interaction and protection mechanism between Li@C60 and nucleic acid bases (NABs): performance of PM6-DH2 on noncovalent interaction of NABs-Li@C60, J. Comp. Chem. 33 (2012) 490–501.
[39] Y. Wang, Theoretical evidence for the stronger ability of thymine to disperse SWCNT than cytosine and adenine: self-stacking of DNA bases vs their cross-stacking with SWCNT, J. Phys. Chem. C 112 (2008) 14297–14305.
[40] E.R. Johnson, S. Keinan, P. Mori-Sanchez, J. Contreras-Garcia, A.J. Cohen, W. Yang, Revealing noncovalent interactions, J. Amer. Chem. Soc. 132 (2010) 6498–6506.
[41] T. Lu, F. Chen, Multiwfn, A multifunctional wavefunction analyzer, J. Compt. Chem. 33 (2012) 580–592.
[42] W. Humphrey, A. Dalke, K. Schulten, VMD: visual molecular dynamics, J. Mol. Graph. 14 (1996) 33–38.